

Supplementary Information

Efficient and durable oxygen reduction and evolution of hydrothermally synthesized $\text{La}(\text{Co}_{0.55}\text{Mn}_{0.45})_{0.99}\text{O}_{3-\delta}$ nanorod/graphene hybrid in alkaline media

Xiaoming Ge,^a F. W. Thomas Goh,^a Bing Li,^a T. S. Andy Hor,^{a,b*} Jie Zhang,^a Peng Xiao,^c Xin Wang,^c Yun Zong,^{a,*} and Zhaolin Liu^{a,*}

a. Institute of Materials Research and Engineering (IMRE), A*STAR (Agency for Science, Technology and Research), 3 Research Link, Singapore 117602, Republic of Singapore.

b. Department of Chemistry, National University of Singapore, 3 Science Drive 3, Singapore 117543, Republic of Singapore.

c. School of Chemical and Biochemical Engineering, Nanyang Technological University, 62 Nanyang Drive, Singapore 637459, Republic of Singapore.

Corresponding authors: zl-liu@imre.a-star.edu.sg (Z. L. Liu); andyhor@imre.a-star.edu.sg (T. S. Andy Hor); y-zong@imre.a-star.edu.sg (Y. Zong).

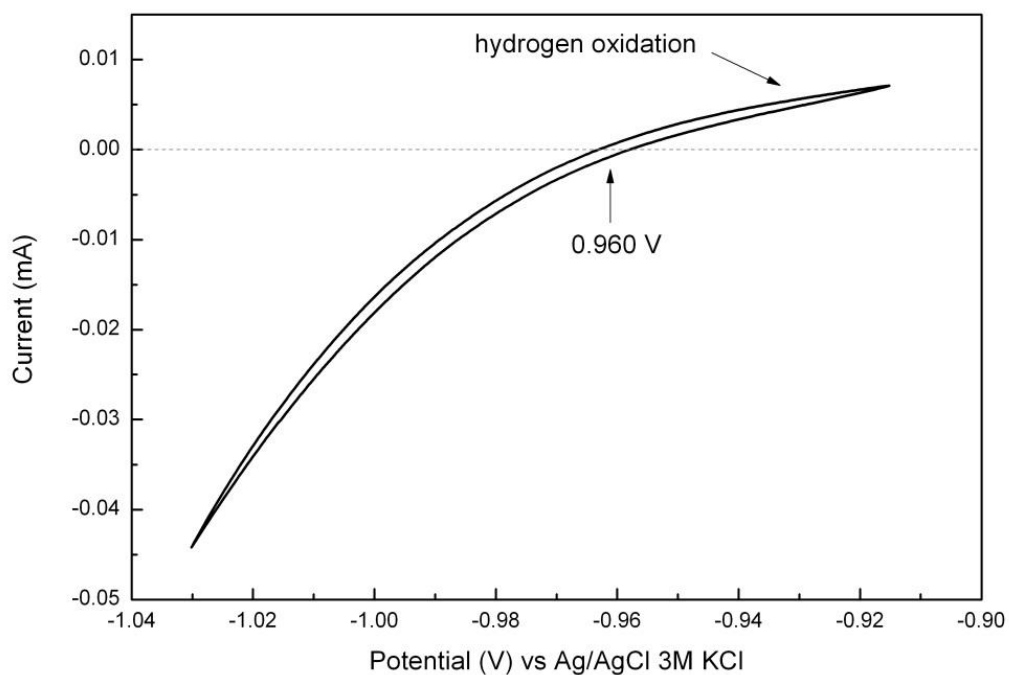


Figure S1. Cyclic voltammetry of a pristine $\Phi 5$ mm Pt rotating-disk electrode (RDE, Metrohm) with Pt foil as counter electrode and Ag/AgCl (3 M KCl) as reference electrode. The potential sweeping rate is 1 mV s^{-1} . The rotating rate of Pt RDE is 2000 rpm. The electrolyte is 99.999% pure H_2 -saturated 0.1 M KOH aqueous solution. According to this figure, the conversion between reversible hydrogen electrode (RHE) and Ag/AgCl (3 M KCl) is denoted as $E(\text{RHE}) = E(\text{Ag/AgCl, 3 M KCl}) + 0.960 \text{ V}$.

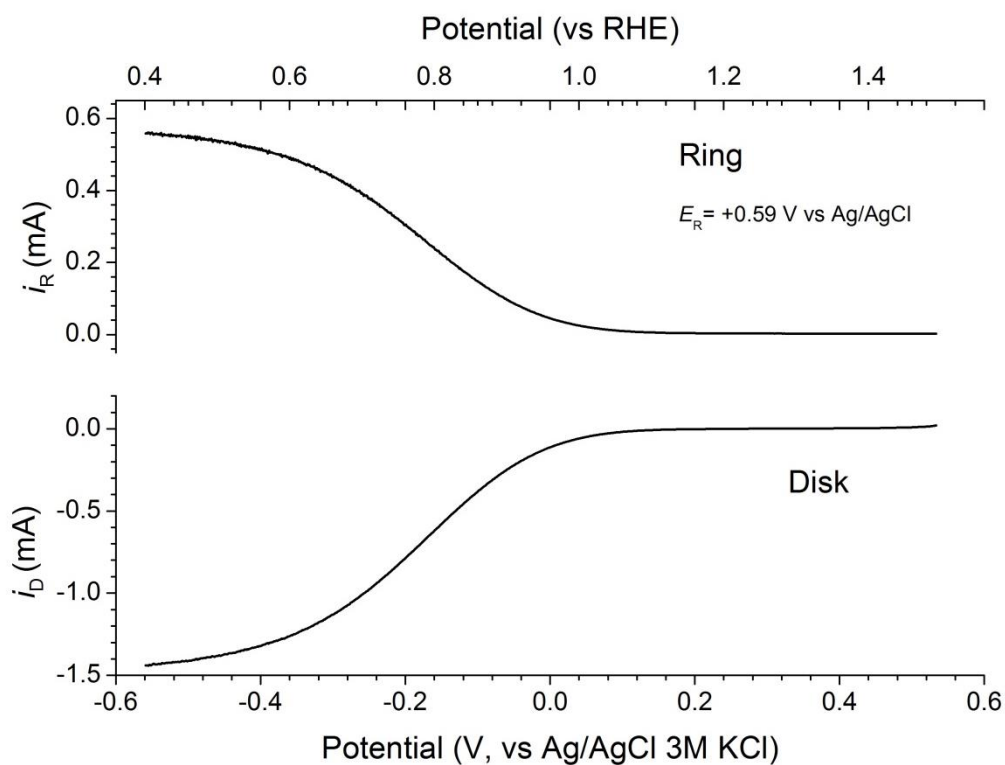


Figure S2. Ring ($\text{Fe}^{2+} \rightarrow \text{Fe}^{3+} + \text{e}^-$) and disk ($\text{Fe}^{3+} + \text{e}^- \rightarrow \text{Fe}^{2+}$) currents for the determination of collection efficiency of RRDE loaded with LCMO/NrGO catalyst. The electrolyte is deaerated 0.1 M NaOH with 0.01 M $\text{K}_3\text{Fe}(\text{CN})_6$. The rotating rate of RRDE is 1600 rpm. The collection efficiency is calculated to be (38.8 ± 0.2) %, close to the manufacture's data 37%.

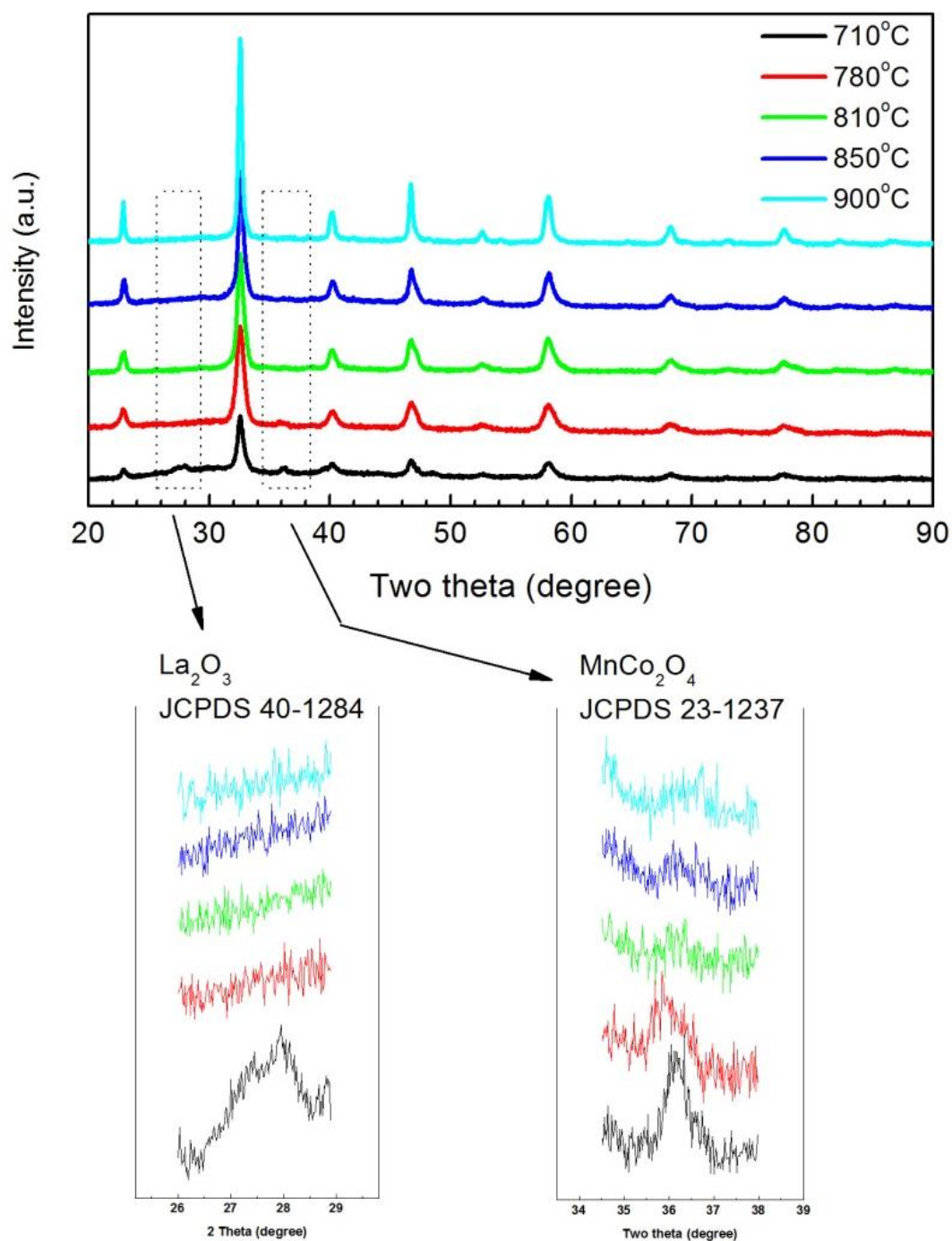


Figure S3. X-ray diffraction (XRD) patterns of LCMO calcined at different temperatures from 710 to 900 °C. LCMO in this work was calcined at 810 °C for the sake of retaining large active sites and eliminating the La_2O_3 and MnCo_2O_4 impurity phases.

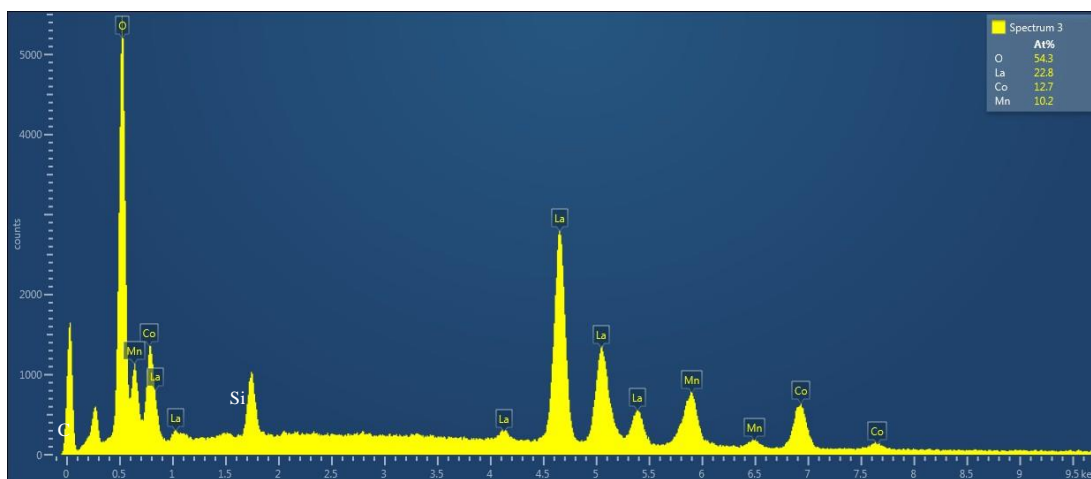


Figure S4. Energy-dispersive X-ray (EDX) spectrum of LCMO. The spectrum was collected from Si wafer supported LCMO, where LCMO particles were dispersed in ethanol, dripped on Si wafer and dried in ambient conditions overnight. The chemical formula of LCMO is $\text{La}(\text{Co}_{0.55}\text{Mn}_{0.45})_{0.99}\text{O}_{3-\delta}$, as derived from this EDX result.

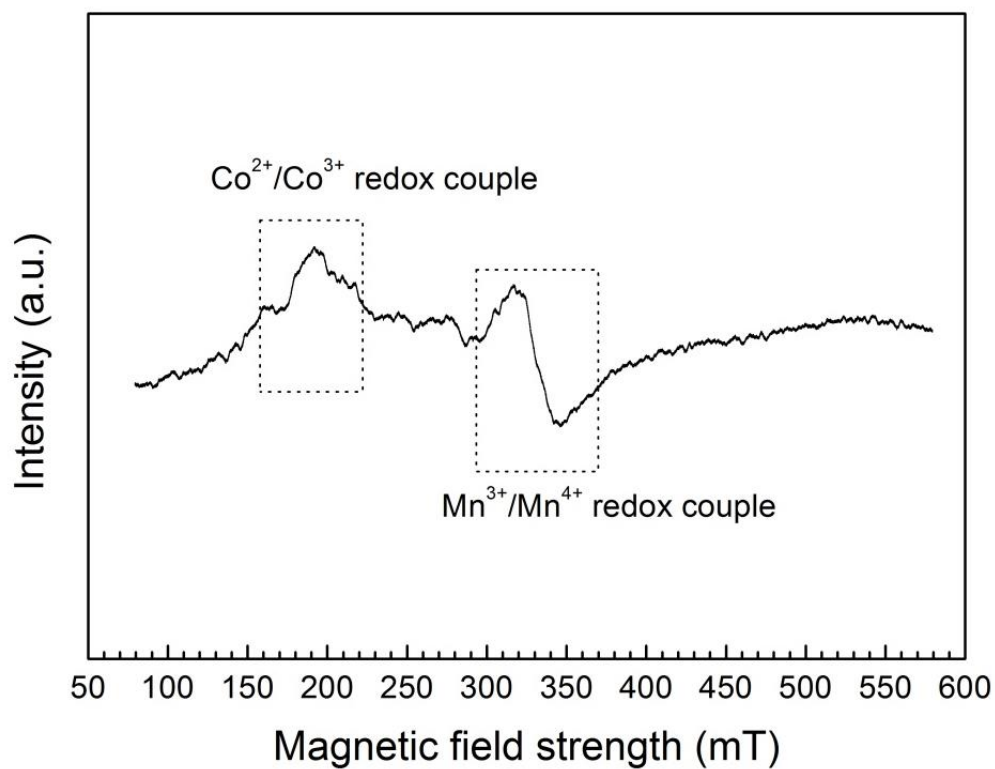


Figure S5. Electron spin resonance (ESR) spectrum of LCMO.

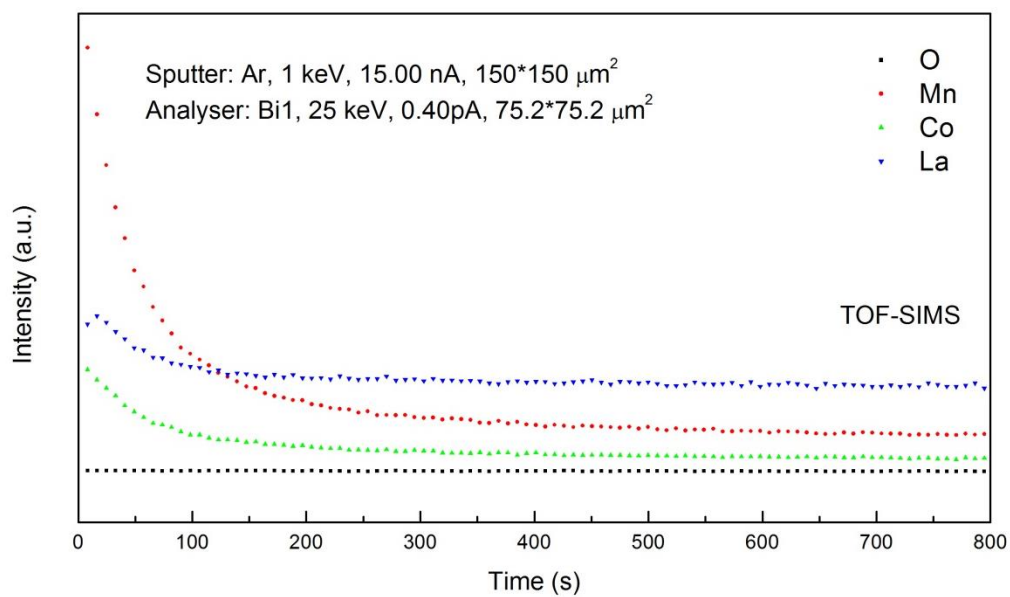


Figure S6. Time-of-flight secondary ion mass spectroscopy (TOF-SIMS) of LCMO. The LCMO powders are dip coated on Si wafer substrate. It is evident from the figure that the surface is rich of Mn.

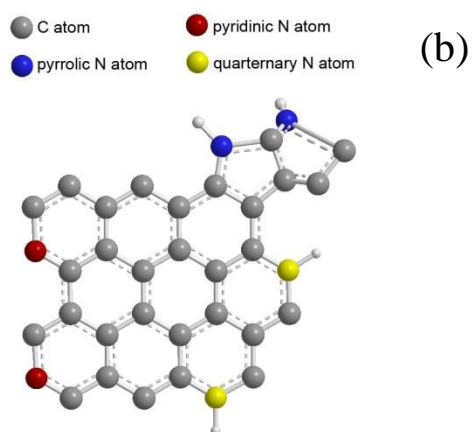
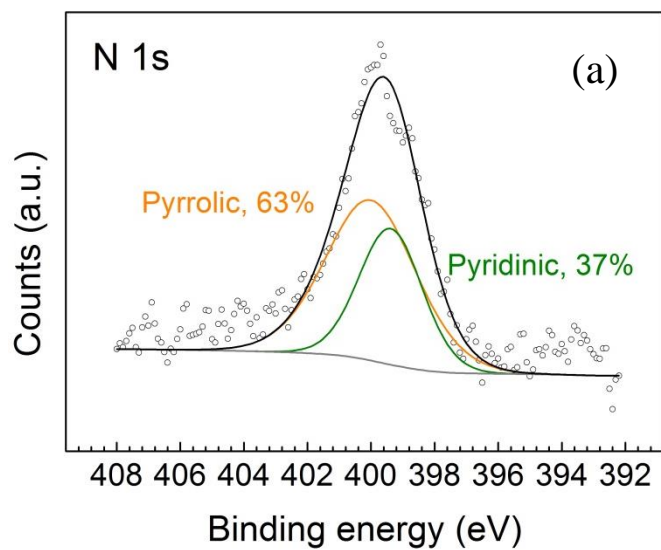


Figure S7. (a) fitted N 1s XPS spectra of NrGO and (b) schematic illustration of nitrogen sites in NrGO.

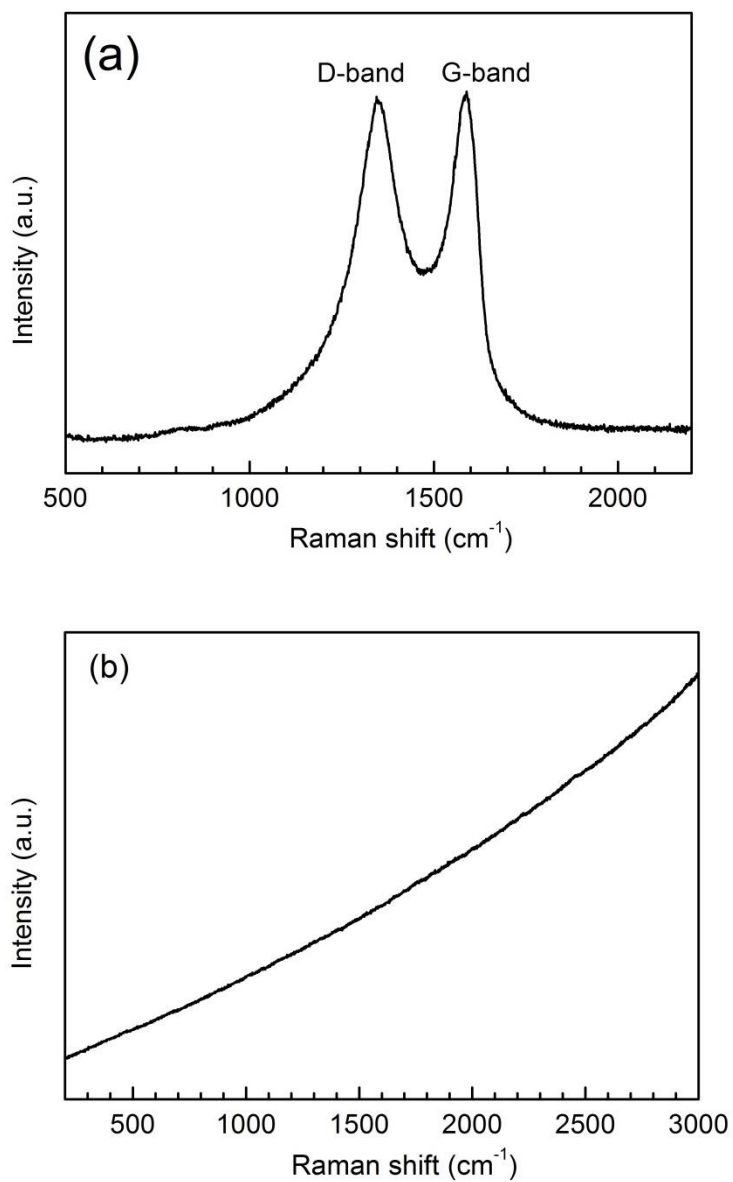


Figure S8. Raman spectra of NrGO (a) and LCMO/NrGO (b). Note that the D-band and G-band of carbon of LCMO/NrGO are screened by the strong fluorescence, which is typical to rare-earth metal oxides such as LCMO.

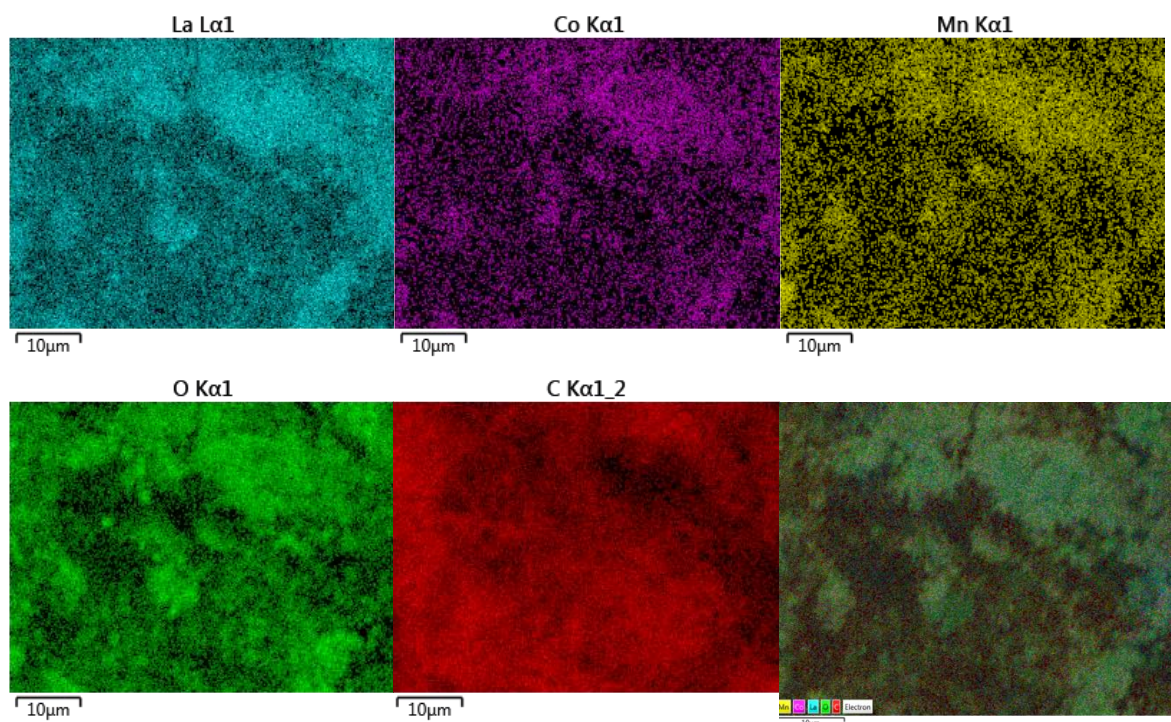


Figure S9. EDX elemental mapping of (a) La $L_{\alpha 1}$, (b) Co $K_{\alpha 1}$, (c) Mn $K_{\alpha 1}$, (d) O $K_{\alpha 1}$, (e) C K_{α} and (f) La-Co-Mn-O-C superimposed images of the LCMO/NrGO hybrid. The EDX mapping shows the LCMO and NrGO are homogeneously distributed in the LCMO/NrGO hybrid catalyst.

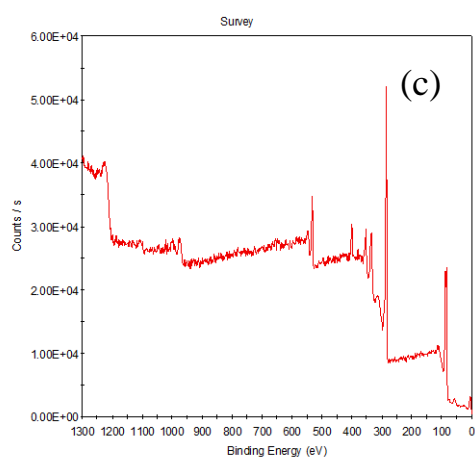
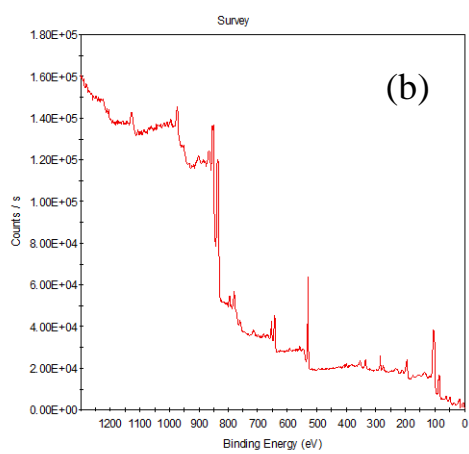
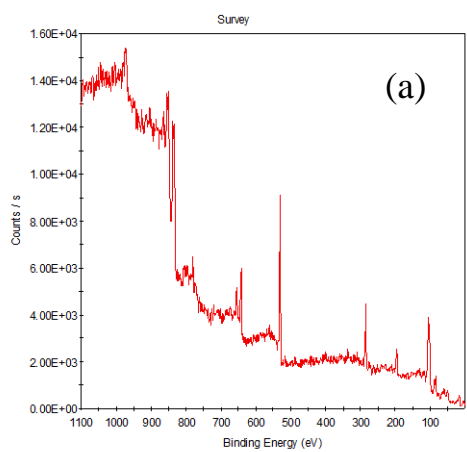


Figure S10. Survey XPS spectra of (a) LCMO/NrGO, (b) LCMO and (c) NrGO.

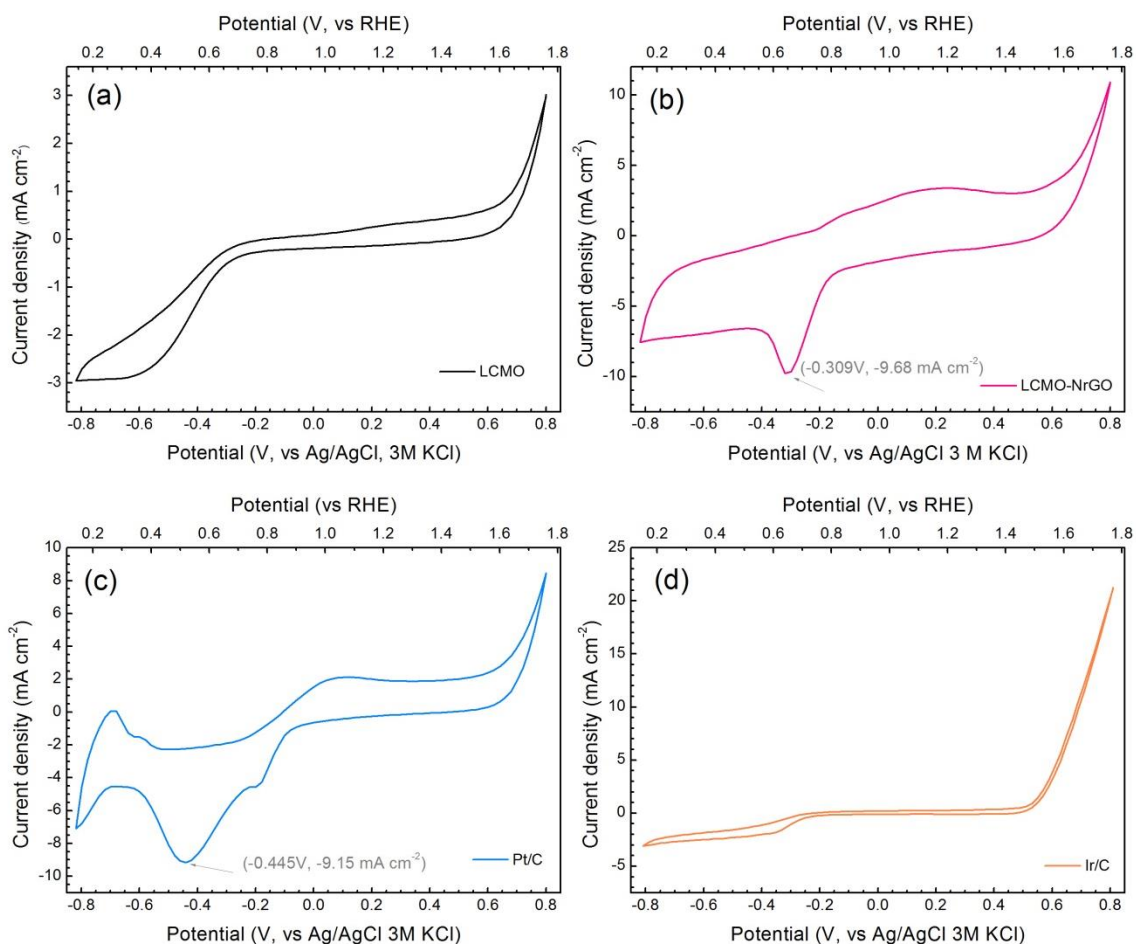


Figure S11. Cyclic voltammograms of (a) LCMO, (b) LCMO/NrGO, (c) Pt/C and (d) Ir/C from the potential range of -0.8 V to 0.8 V in O₂-saturated 0.1 M KOH solution. The full range CVs cover both the ORR and the OER regions.

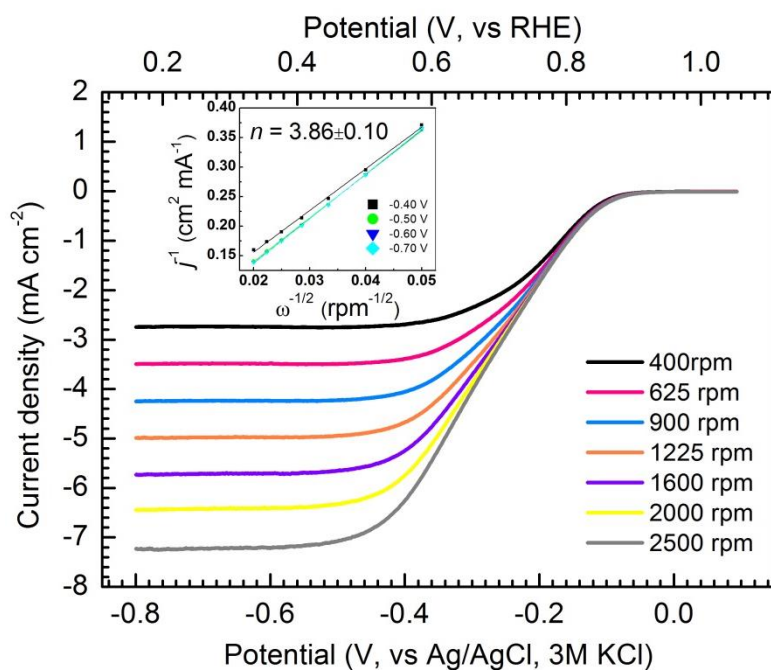


Figure S12. ORR polarization curves of mechanically mixed LCMO and NrGO (LCMO+NrGO) loaded on glassy carbon RDE in O₂-saturated 0.1 M KOH at rotating rates from 400 to 2500 rpm. The inset shows the corresponding K–L plots at potentials from -0.50 V to -0.80 V. The electrolyte is O₂-saturated 0.1 M KOH solution.

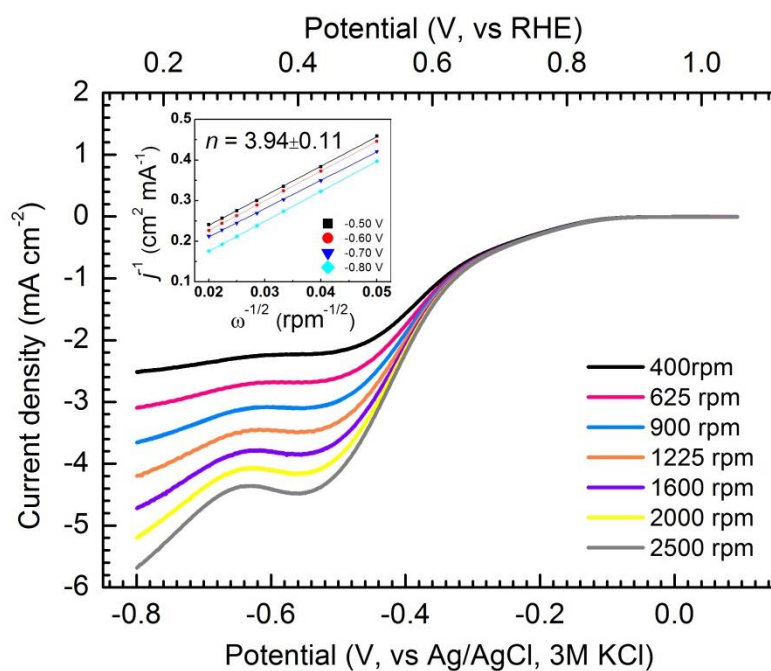


Figure S13. ORR polarization curves of LCMO loaded on glassy carbon RDE in O_2 -saturated 0.1 M KOH at rotating rates from 400 to 2500 rpm. The inset shows the corresponding K–L plots at potentials from -0.50 V to -0.80 V. The electrolyte is O_2 -saturated 0.1 M KOH solution.

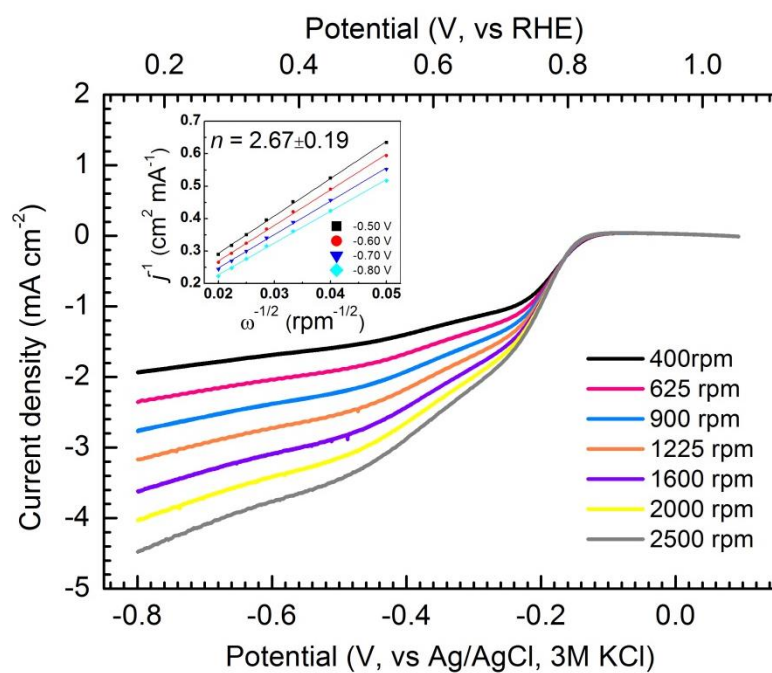


Figure S14. ORR polarization curves of NrGO loaded on glassy carbon RDE in O₂-saturated 0.1 M KOH at rotating rates from 400 to 2500 rpm. The inset shows the corresponding K–L plots at potentials from -0.50 V to -0.80 V. The electrolyte is O₂-saturated 0.1 M KOH solution.

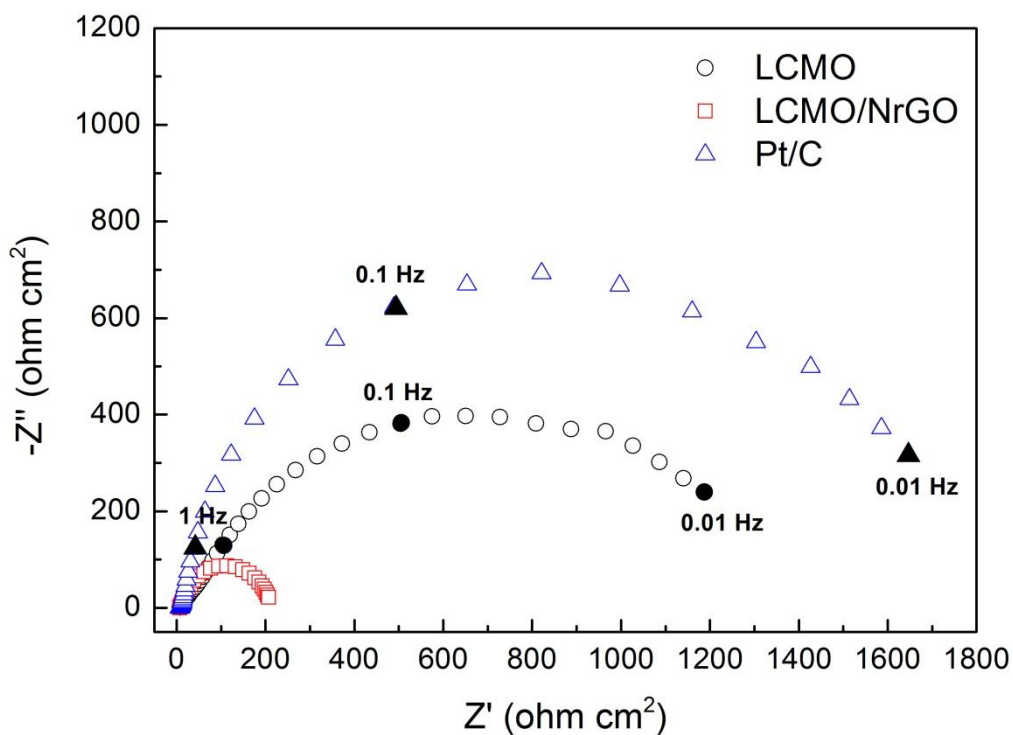


Figure S15. Impedance spectra of LCMO/NrGO, LCMO and Pt/C under an OER polarization condition of 0.6 V vs Ag/AgCl. The catalysts were loaded on glass carbon RDE under a rotating rate of 400 rpm. As indicated from the figure, LCMO/NrGO shows the smallest polarization resistance for OER while the ohmic resistance for RDE loaded with the three catalysts are almost identical. The electrolyte is O_2 -saturated 0.1 M KOH solution.

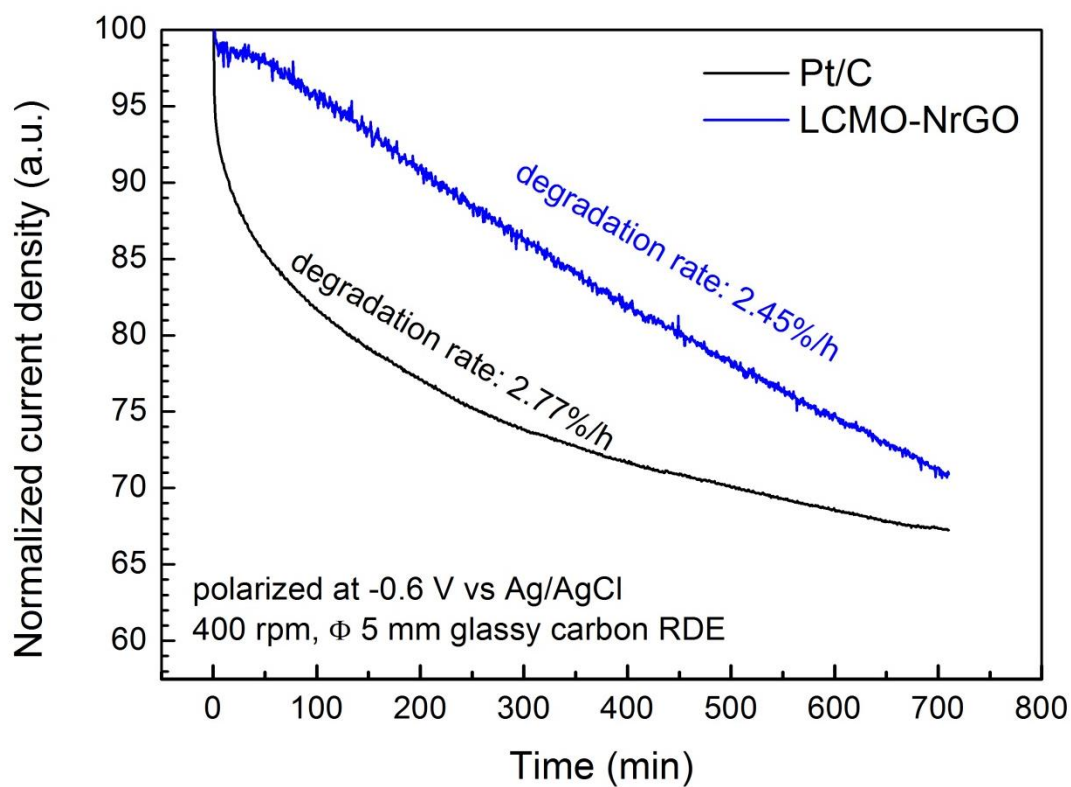


Figure S16. Chronoamperometric curves of LCMO/NrGO-loaded and Pt/C-loaded carbon fibre paper air cathodes. The chronoamperometry was run in a three-electrode configuration with Pt foil as counter electrode. Both air cathodes were polarized at -0.60 V vs Ag/AgCl. The electrolyte was O₂-saturated 0.1 M KOH solution.

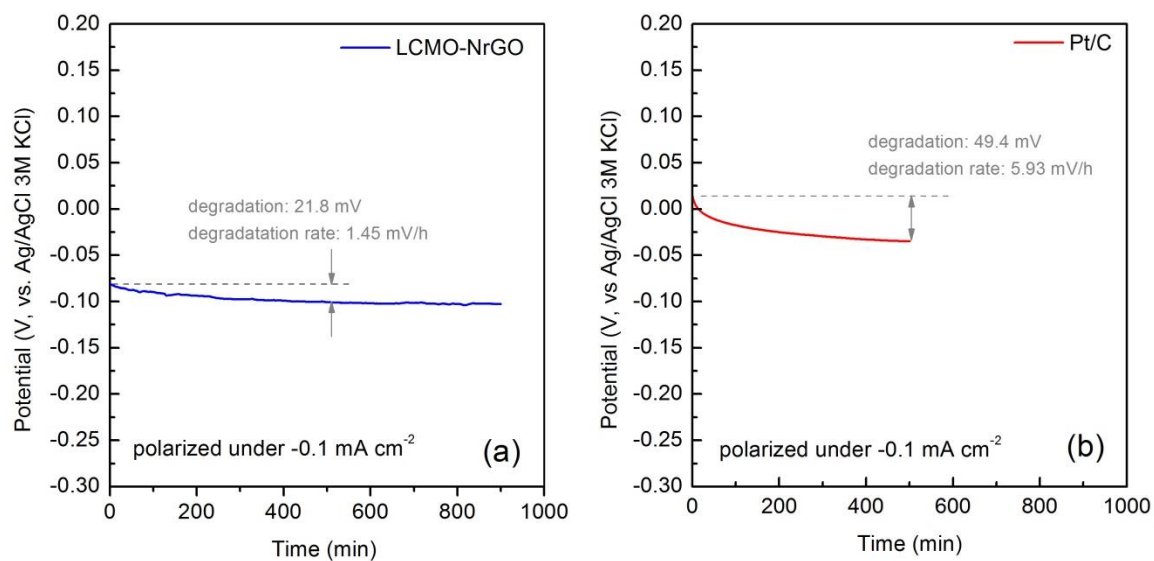


Figure S17. Chronopotentiometric curves of LCMO/NrGO (a) and Pt/C (b) loaded on $\Phi 5$ mm glassy carbon RDE electrodes. The working electrodes are polarized under -0.1 mA cm^{-2} , in ORR mode. The rotating rate is 400rpm. The electrolyte is O_2 -saturated 0.1 M KOH.

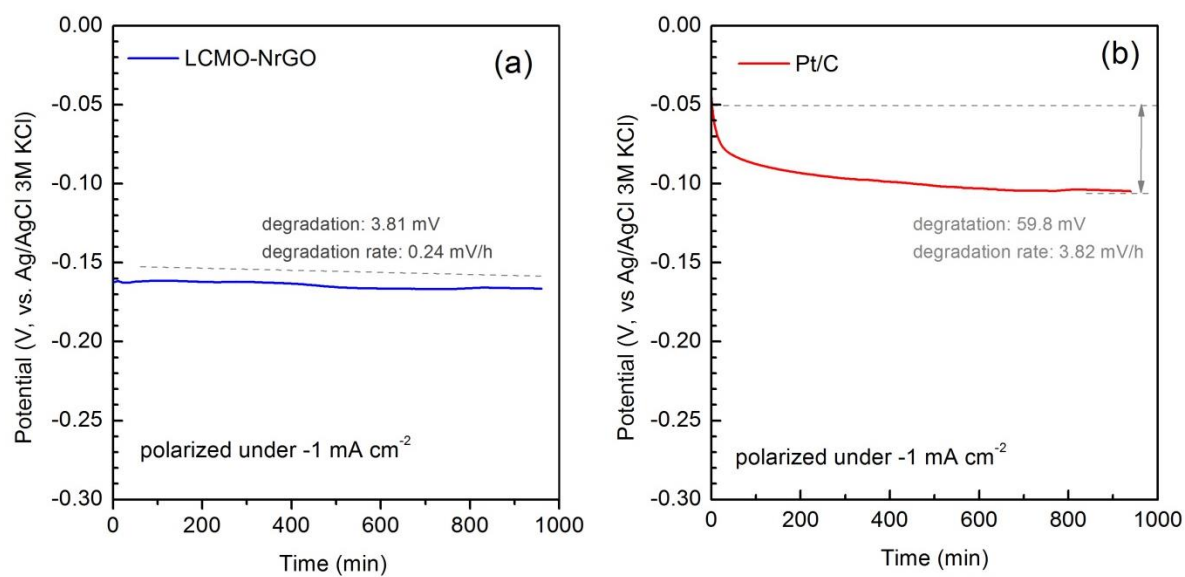


Figure S18. Chronopotentiometric curves of LCMO/NrGO (a) and Pt/C (b) loaded on $\Phi 5\text{mm}$ glassy carbon RDE electrodes. The working electrodes are polarized under -1 mA cm^{-2} , in ORR mode. The rotating rate is 400rpm. The electrolyte is O_2 -saturated 0.1 M KOH.

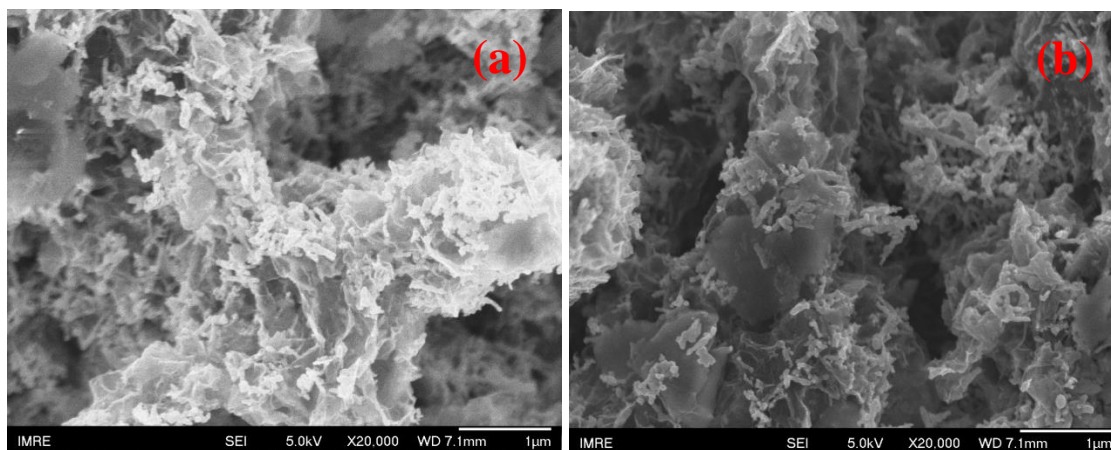


Figure S19. Field-emission scanning electron microscopy (FE-SEM) of LCMO/NrGO catalyst loaded on glassy carbon RDE before (a) and after (b) chronopotentiometry degradation under a current density of -1 mA cm^{-2} , rotating rate of 400 rpm and time of 16 hours.

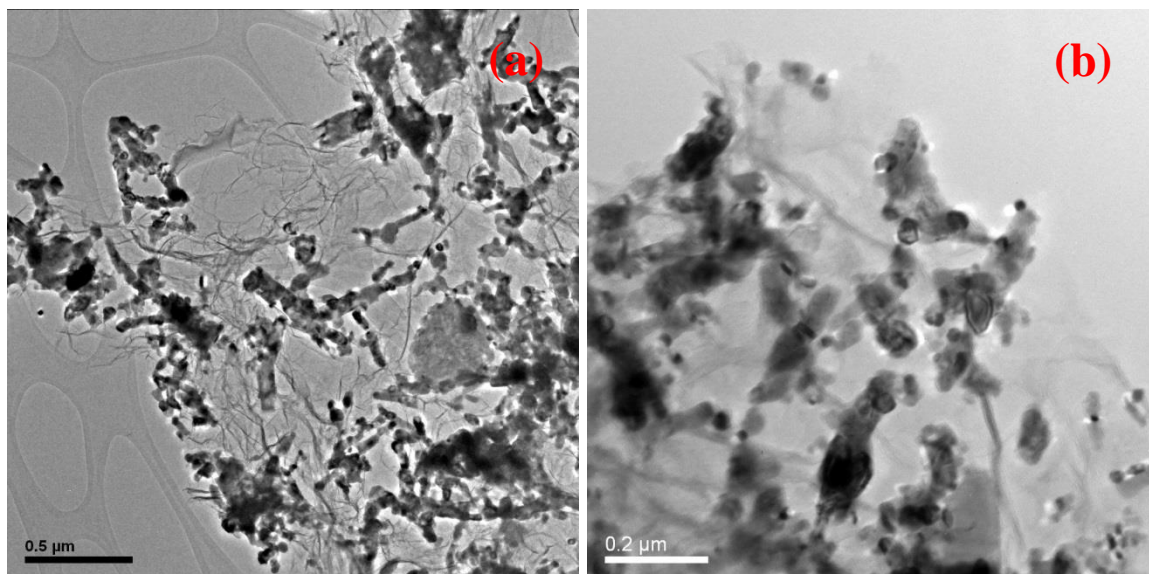


Figure S20. Transmission electron microscopy (TEM) morphology images of LCMO/NrGO before (a) and after (b) chronopotentiometry degradation, a current density of -1 mA cm^{-2} , rotating rate of 400 rpm and time of 16 hours. The catalyst after degradation test was removed RDE tip by ultrasonication in ethanol, and loaded on Cu mesh.

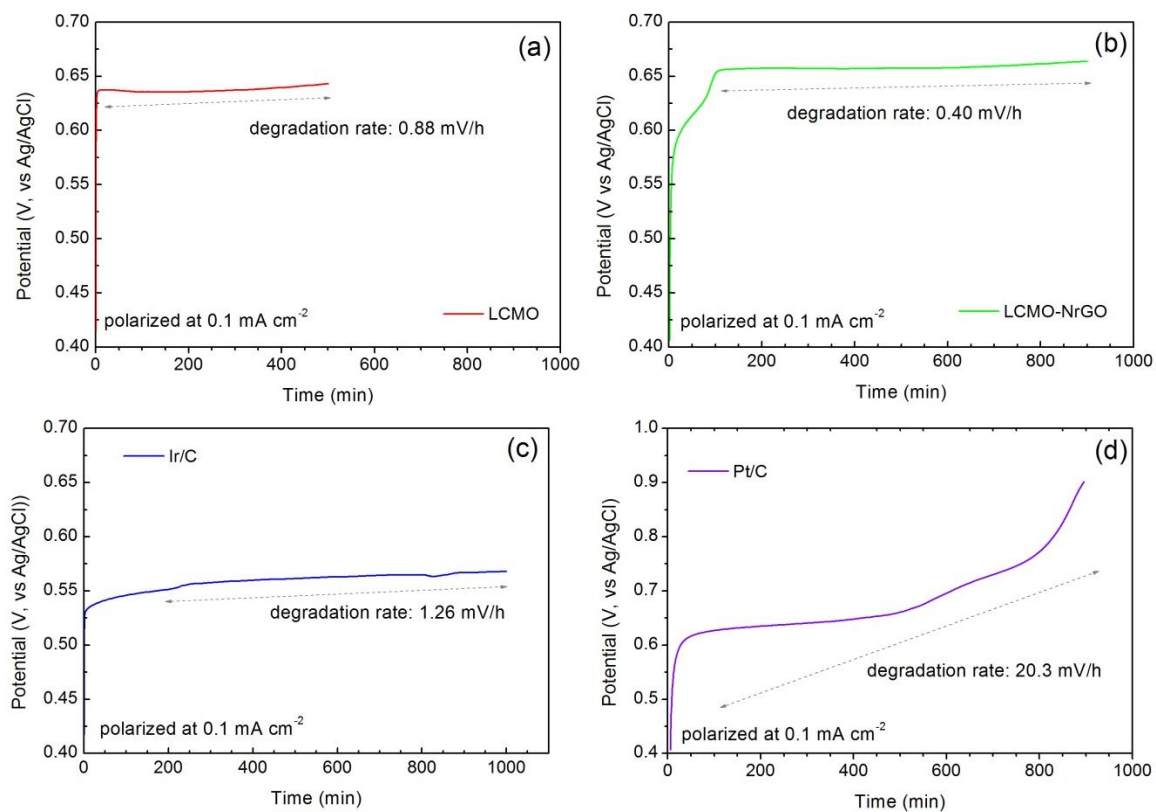


Figure S21. Chronopotentiometric curves of LCMO (a), LCMO/NrGO (b), Ir/C (c) and Pt/C (d) loaded on $\Phi 5\text{mm}$ glassy carbon RDE electrodes. The working electrodes are polarized under 0.1 mA cm^{-2} , in OER mode. The rotating rate is 400rpm. The electrolyte is O_2 -saturated 0.1 M KOH .

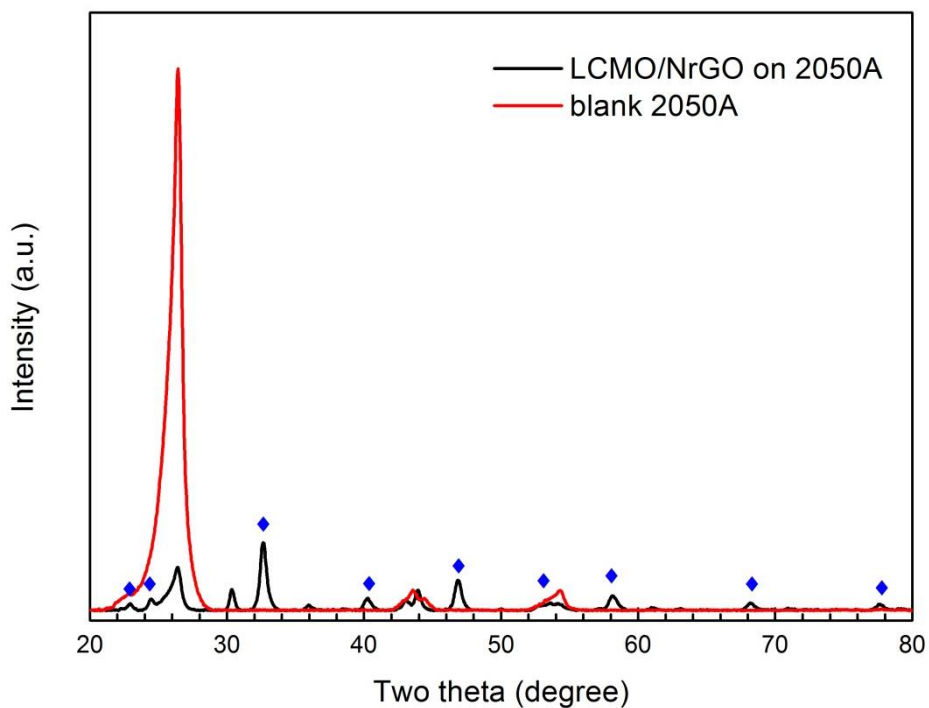


Figure S22. X-ray diffraction (XRD) patterns of LCMO/NrGO air cathode after a chronopotentiometry degradation, under a current density of -10 mA cm^{-2} , rotating rate of 400 rpm, and time of 16 hours. The air cathode was prepared by anchoring LCMO/NrGO catalyst on 2050A carbon paper by Nafion. The blank 2050A carbon paper is incorporated for a comparison purpose. The blue diamond symbol (\diamond) corresponds to the perovskite LCMO.

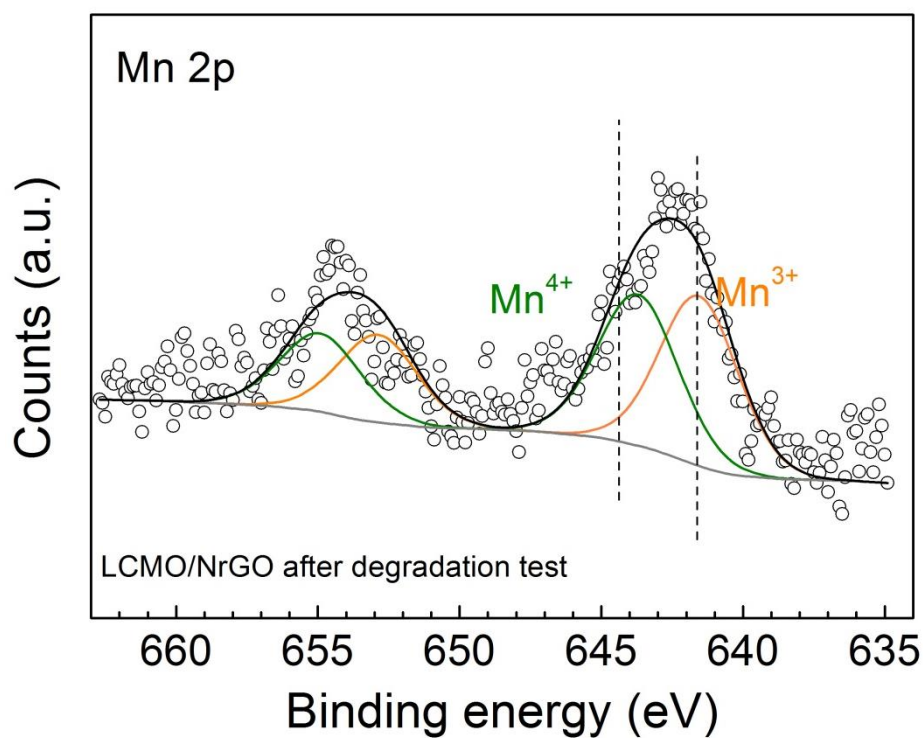


Figure S23. X-ray photoelectron spectrum of Mn 2p doublet of LCMO/NrGO air cathode before (a) and after (b) chronopotentiometry degradation, under a current density of -10 mA cm^{-2} , rotating rate of 400 rpm, and time of 16 hours. The air cathode was prepared by anchoring LCMO/NrGO catalyst on 2050A carbon paper by Nafion.

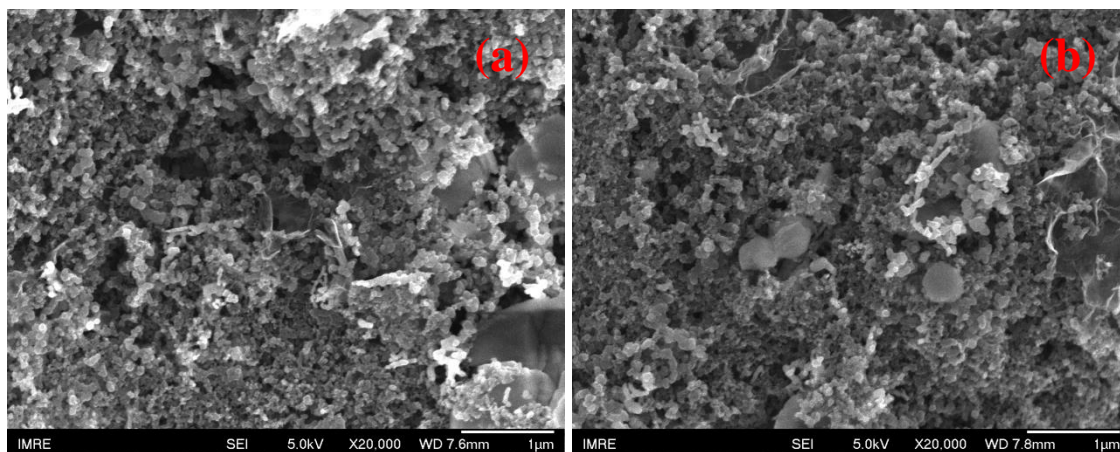


Figure S24. Field-emission scanning electron microscopy (FE-SEM) of LCMO/NrGO air cathode before (a) and after (b) chronopotentiometry degradation, under a current density of -10 mA cm^{-2} , rotating rate of 400 rpm, and time of 16 hours. The air cathode was prepared by anchoring LCMO/NrGO catalyst on 2050A carbon paper by Nafion.

Table S1. Determination of e_g electrons of $\text{La}(\text{Co}_{0.55}\text{Mn}_{0.45})_{0.99}\text{O}_{3-\delta}$ (LCMO).

	Co		Mn	
Valence	Co^{2+}	Co^{3+}	Mn^{3+}	Mn^{4+}
spin state	high spin ¹	intermediate spin ²	high spin ³	N.A.
assignment	$t_{2g}^5 e_g^2$	$t_{2g}^5 e_g^1$	$t_{2g}^3 e_g^1$	$t_{2g}^3 e_g^0$
Composition ⁴	59 at. %	41 at. %	31 at. %	69 at. %
Assignment of LCMO	$t_{2g}^{4.12} e_g^{1.03}$			

1: M. C. Viola, M. J. Martinez-Lope, J. A. Alonso, J. L. Martinez, J. M. De Paoli, S. Pagola, J. C. Pedregosa, M. T. Fernandez-Diaz, and R. E. Carbonio, *Chem. Mater.*, 2003, **15**, 1655-1663.; A. P. Sazonov, I. O. Troyanchuk, M. Kopcewicz, V. V. Sikolenko, U. Zimmermann, and K. Barner, *J. Phys.: Condens. Matter*, 2007, **19**, 046218.

2: J. Q. Yan, J. S. Zhou and J. B. Goodenough, *Phys. Rev. B*, 2004, **69**, 134409. ; M. A. Korotin, S. Yu. Ezhov, I. V. Solovyev, and V. I. Anisimov, *Phys. Rev. B*, 1996, **54**, 5309-5316.; P. G. Radaelli, S. W. Cheong, *Phys. Rev. B*, 2002, **66**, 094408.; K. Asai, A. Yoneda, O. Yokokura, J. M. Tranquada, G. Shirane, and K. Kohn, *J. Phys. Soc. Jpn.*, 1998, **67**, 290-296.

3: J. Blasco, J. Garcia, J. M. de Teresa, M. R. Ibarra, J. Perez, P. A. Algarabel, C. Marquina and C. Ritter, *Phys. Rev. B*, 1997, **55**, 8905-8910.; T. A. Tyson, Q. Qian, C. C. Kao, J. P. Rueff, F. M. F. de Groot, M. Croft, S. W. Cheong, M. Greenblatt, and M. A. Subramanian, *Phys. Rev. B*, 1990, **60**, 4665-4674.; C. Autret, J. Hejtmanek, K. Knizek, M. Marysko, Z. Jirak, M. Dlouha, S. Vratilav, *J. Phys.: Condens. Matter*, 2005, **17**, 1601-1616.

4: Based on the XPS results, this work.

Table S2. Chemical states of Mn, Co and La in LCMO/NrGO and LCMO.

	Mn 2p _{3/2}			Co 2p _{3/2}			Mn/Co ratio	La 3d _{5/2}		(Co+Mn)/La ratio
	Mn ³⁺ (eV)	Mn ⁴⁺ (eV)	Mn ³⁺ content (%)	Co ²⁺ (eV)	Co ³⁺ (eV)	Co ²⁺ content (%)		Main (eV)	Satellite (eV)	
LCMO/NrGO	641.6	642.9	40.8	780.0	781.2	58.7	4.42	834.1	838.3	1.17
LCMO	641.6	642.7	21.6	779.7	781.1	63.8	2.67	833.9	838.3	1.41

Table S3. Binding energies of light elements in LCMO/NrGO, LCMO and NrGO.

	O 1s			C 1s			N 1s	
	Scan A	Scan B	Scan C	Scan A (C=C)	Scan B (C=N)	Scan C (C-N)	Pyrrolic	Pyridinic
LCMO/NrGO	529.3	530.9	532.3	284.5	285.7	288.2	399.7	398.2
NrGO	–	531.1	533.0	284.6	285.4	288.3	400.0	399.4
LCMO	529.4	531.2	–	–	–	–	–	–

Table S4. Comparison of the potential gap (ΔE) between ORR and OER of various bifunctional catalysts from literature in O₂-saturated 0.1 M KOH aqueous solution.

Catalysts	ORR $E@j=-3$ mA cm ⁻² [V]	OER $E@j=10$ mA cm ⁻² [V]	ΔE (OER– ORR) [V]	References
LCMO/NrGO	-0.178 (0.782)*	0.782 (1.742)	0.960	This work
LCMO+NrGO	-0.251 (0.709)	NA	NA	
20 wt.% Ir/C	-0.348 (0.612)	0.738 (1.698)	1.086	
30 wt.% Pt/C	-0.167 (0.793)	NA	NA	
MnO _x on glassy carbon	0.73	1.77	1.04	Gorlin and Jaramillo, <i>J. Am. Chem. Soc.</i> , 132 (2010) 13612.
20 wt.% Pt/C	0.86	2.02	1.16	
MnCoFeO ₄ /NrGO	0.78	1.71	0.93	Zhan et al., <i>J. Mater. Chem. A</i> , 2 (2014) 16217.
MnCoFeO ₄ /C	0.59	1.71	1.12	
Co _{1.5} Fe _{1.5} O ₄ /C	0.38	1.69	1.31	
Mn _{1.5} Fe _{1.5} O ₄ /C	0.66	1.80	1.14	
RuO ₂ /C	0.68	1.62	0.94	Wang et al., <i>Nanoscale</i> , 5 (2013) 5312.
Co ₃ O ₄ /2.7Co ₂ MnO ₄	0.68	1.77	1.09	
Co ₃ O ₄	0.49	1.83	1.34	
Co ₂ MnO ₄	0.59	1.92	1.33	
Co ₃ O ₄ + Co ₂ MnO ₄	0.55	1.86	1.31	Hardin et al., <i>J. Phys. Chem. Lett.</i> , 4 (2013) 1254.
ns-LaNiO ₃ /NC	0.64	1.66	1.02	

* The values in parenthesis are converted from Ag/AgCl scale to RHE scale according to Figure S1, $E_{\text{RHE}} = E_{\text{Ag/AgCl}} + 0.960$ V.